

Improving the efficiency of gas turbine systems with volumetric solar receivers



Fontina Petrakopoulou*, Sergio Sánchez-Delgado, Carolina Marugán-Cruz, Domingo Santana

Thermal and Fluids Engineering Department, Universidad Carlos III de Madrid, Avda. de la Universidad 30, 28911 Leganés (Madrid), Spain

ARTICLE INFO

Keywords:

Exergy analysis
Solar energy
Volumetric solar receiver
Gas turbines
Combined-cycle power plant
Hybrid plants

ABSTRACT

The combustion process of gas turbine systems is typically associated with the highest thermodynamic inefficiencies among the system components. A method to increase the efficiency of a combustor and, consequently that of the gas turbine, is to increase the temperature of the entering combustion air. This measure reduces the consumption of fuel and improves the environmental performance of the turbine. This paper studies the incorporation of a volumetric solar receiver into existing gas turbines in order to increase the temperature of the inlet combustion air to 800 °C and 1000 °C. For the first time, detailed thermodynamic analyses involving both energy and exergy principles of both small-scale and large-scale hybrid (solar-combined cycle) power plants including volumetric receivers are realized. The plants are based on real gas turbine systems, the base operational characteristics of which are derived and reported in detail. It is found that the indications obtained from the energy and exergy analyses differ. The addition of the solar plant achieves an increase in the exergetic efficiency when the conversion of solar radiation into thermal energy (i.e., solar plant efficiency) is not accounted for in the definition of the overall plant efficiency. On the other hand, it is seen that it does not have a significant effect on the energy efficiency. Nevertheless, when the solar efficiency is included in the definition of the overall efficiency of the plants, the addition of the solar receiver always leads to an efficiency reduction. It is found that the exergy efficiency of the combustion chamber depends on the varying air-to-fuel ratio and, in most cases, it is maximized somewhere between the applied inlet combustion air temperatures of 800 °C and 1000 °C.

1. Introduction

In recent years, the international community has focused its efforts on the development and better understanding of the hybridization of solar energy with conventional power plants. The main motivation of this is to decrease the cost of electricity, as well as to promote regional energy independence, reduce CO₂ emissions and increase the standard of living of a society [1]. The wider development of technologies based on solar energy from the 1980s until today has led to hybridization proposals of several concentrated solar power (CSP) technologies. CSP technologies include parabolic trough, solar tower, volumetric receiver, fresnel or dish [2]. The most suitable technology depends on the project, since parameters like the direct normal irradiance, climate conditions, and space availability have to be taken into account.

Until today, most solar thermal plants have been coupled with steam cycles achieving efficiencies of about 42%. This kind of power plant hybridization facilitates minimal modification to the original design of a power plant [3]. However, the coupling of solar plants with gas turbines results in a significantly higher total efficiency [4,5]. There

are two main ways to couple solar plants with conventional power plants: either by using the solar energy in the heat recovery steam generator (HRSG) or, if applicable, in the gas turbine (GT) system of the plant.

Several studies related to the hybridization of parabolic trough collectors and volumetric receivers with conventional power plants can be found in literature. Nevertheless, the published works use energy analysis to compare and evaluate energy systems that may lead to misleading conclusions. In the present paper exergy analysis is used as the main evaluation tool of newly proposed hybrid systems. Furthermore, different definitions of the efficiency that can lead to significantly contrasting results among different research studies are discussed.

Antonanzas et al. (2014) [1] analyzed the overall potential for solar thermal integration in 51 combined-cycle gas turbines (CCGTs) in Spain under different operational scenarios. They found that when the air temperature increases, the efficiency of the power plant decreases, while in these periods, the direct normal irradiation (DNI) is higher. Therefore, the hybridization of a combined cycle with a solar plant can

* Corresponding author.

E-mail address: fpetrako@ing.uc3m.es (F. Petrakopoulou).

Nomenclature		tot	overall system
\dot{E}	exergy rate (MW)	<i>Greek symbols</i>	
\dot{m}	mass flow rate (kg/s)	ε	exergy efficiency
\dot{Q}	thermal energy rate (MW)	η	energy efficiency
r	distance to the tower (km)	θ	incidence angle
\dot{W}	power (MW)	<i>Abbreviations</i>	
<i>Subscripts</i>		CC	combined cycle
<i>at</i>	attenuation	COMP	compressor
<i>bl</i>	blocking	CSP	concentrating solar power
<i>D</i>	exergy destruction	DNI	direct normal irradiation
<i>F</i>	fuel (exergy)	GT	gas turbine
<i>hel</i>	heliostats	HRSG	heat recovery steam generator
<i>int</i>	intercepted	ISCC	integrated solar combined cycle
<i>k</i>	component	LCOE	levelized cost of electricity
<i>L</i>	loss (exergy)	NG	natural gas
<i>P</i>	product (exergy)	pp	percentage points
<i>ref</i>	reflected	ST	steam turbine
<i>s</i>	shading		

be used to alleviate the production drop. However, it is not possible to define a specific way for the integration, due to the different operational conditions and locations of the conventional plants. Amelio et al. (2014) [4] evaluated the performance of an integrated solar combined-cycle power plant in Spain (Almería), where parabolic collectors were used to heat up the air entering the combustion chamber of the GT. Once the air was compressed, it flowed through the parabolic collector to be heated with solar energy. To compare the power plant efficiency, with or without solar energy, three expressions for the efficiency were defined. One definition included the solar power available to the collectors; another definition included only the thermal power generated by the collectors, while the last definition excluded the solar energy input. The study showed that the net average annual efficiency of the plant was higher in comparison with the reference combined-cycle efficiency without solar integration, for all efficiency definitions. Alqahani et al. (2016) [6] studied integrated solar combined-cycle power plants (ISCCs), comprised of a CSP plant (with parabolic trough system an oil as the heat transfer fluid) and a natural gas-fired combined-cycle power plant. The authors compared the levelized cost of electricity (LCOE) of four power plants: standalone CSP, concentrated solar power with energy storage, standalone natural gas combined cycle and ISCC. The authors concluded that the ISCC can reduce the LCOE in comparison with the other hybrid or renewable plants. Saghafifar and Gadalla [7] investigated the hybridization of a 50 MW-power plant with a solar plant involving a volumetric solar receiver in the United Arab Emirates and optimized it thermo-economically. The optimization included several important parameters of the power plant, such as the inlet temperature of the GT system and the pressure ratios of the turbines. It was concluded that the installment of a new hybrid power plant would be more economical than the hybridization of the already existing plant.

Another type of a CSP plant used in hybridization scenarios with ISCCs includes an air receiver that can be either tubular [8] or volumetric [9,10]. A review of solar volumetric receivers can be found in [11]. Spelling et al. [12] developed a dynamic model to determine the thermodynamic and economic performance of a solar combined cycle power plant. The receiver consisted of an open volumetric receiver, where the solar radiation was concentrated in porous ceramic foam. The temperature of the air was increased in contact with the porous material and a packed-bed volumetric air storage unit was used to stabilize the air temperature. The authors found that this hybridization could compete with current solar thermal technologies, in terms of

LCOE, depending on the magnitude of the initial investment.

Several different designs for the volumetric receiver can be found in literature. In 2006 Heller et al. [13] presented the results of an experimental prototype solar powered gas-turbine system installed in Plataforma Solar de Almería in Spain in 2002. A solar receiver cluster able to provide pressurized air at 1000 °C was developed in the framework of the project SOLGATE. This temperature was higher than the 800 °C previously achieved at a pressure of 15 bar by researchers of the German Aerospace Center (DLR) [10]. The air is directly introduced into the combustion chamber of the gas cycle, using a by-pass to control the temperature of the air at the inlet of the combustion chamber. Heller et al. described the configuration of the plant, the component efficiencies and the operation experience, during the successful test of the solar GT for 100 h of operation. Pozivil et al. (2013) [14] also developed a pressurized air-based solar receiver for power generation in GTs. This work presented two prototypes of a solar receiver of 3 kW_{th} and 35 kW_{th}. The use of this receiver allowed the heating of pressurized air in the range of 4–30 bar and 800–1200 °C. The analysis of the volumetric receiver and its integration into a GT showed that the power cycle efficiency increased with higher turbine inlet temperature. On the other hand, the efficiency of the solar receiver decreased at a higher operating temperature, due to the radiation losses. The thermal receiver efficiency was defined as the ratio between the thermal power absorbed by the air flowing through the solar receiver over the concentrated solar flux incident on receiver aperture.

In 2015, del Río et al. [15], based on previous work realized in the framework of the projects REFOS and SOLGATE, worked on the project SOLTREC, where they studied the development and manufacturing of a volumetric receiver for gas-turbine integration. The developed volumetric receiver with a diameter of 1500 mm and thermal power of 1.47 MW_{th} was able to heat up the air to 1000 °C (with solar shares up to 80%). The quartz window of the SOLTREC receiver was an improved version of that of the SOLGATE. With this new prototype, the authors studied the performance and cost reduction potential of the SOLTREC receiver. In 2016, Korzynietz et al. [8] presented the obtained results of the first megawatt scale solar-hybrid plant (SOLUGAS project) with a solarized GT in San Lucar la Mayor (Spain) operated for more than 1000 h. The solar receiver was designed using metallic tubular receiver technology and reached temperatures up to 800 °C. The plant used the GT system MercuryTM 50 of 4.6 MW with an efficiency of 39% and 69 heliostats. The air was preheated up to 800 °C in the solar receiver, and then, if necessary, cooled down to the maximum temperature tolerable

at the inlet of the combustion chamber with the use of a by-pass. The authors, defined the receiver thermal efficiency as the ratio of the energy absorbed by the air through the solar receiver to the input power into the aperture of the receiver. They obtained values of solar receiver efficiencies close to 80% at different operational conditions. These efficiencies are directly related with the cost of the plant, particularly that of the solar field. Therefore, the authors proposed as objective for a commercial system, a minimum receiver efficiency of 80%. They also proposed to focus the research effort on the development of a combustor allowing up to 1000 °C inlet temperature.

The study presented in this article focuses on the hybridization of novel solar plants incorporating pressurized volumetric receivers with conventional natural gas combined-cycle power plants, where solar energy is used to preheat compressed air in GTs. The examined natural gas plants involve three small-scale and two large-scale power plants. All of the gas turbine models used are based on commercial models. The goal is to reduce the natural gas consumption and improve the environmental performance of the turbines and overall plants. For the first time, a study evaluating and comparing hybrid solar-combined cycle power plants with volumetric receivers is realized using both exergy and energy principles. The use of exergy analysis allows the accurate comparison of the plants with increasing combustion temperature, not possible with energy analysis. The optimal hybridization scenarios with increased efficiencies are discussed in detail.

2. Power plant simulations

The power plants studied in this work are simulated using the commercial software EbsilonProfessional [16]. The three small-scale gas-turbine systems (4–10 MW) incorporate the following GT systems: solar Mercury 50, Mars100 and GE10-1 [17–19]. All gas turbine systems are simulated in detail by being split into their three main components: compressor, combustion chamber and expander. Operational input parameters of the first two turbines are derived from the gas-turbine library incorporated in EbsilonProfessional, as well as selected Refs. [20,21]. Specific data for GE10-1 are extrapolated using information provided by the manufacturer [18]. The flow diagrams of the base gas-turbine systems and their derived operational specifications are presented in Fig. 1 and Tables 1 and 2.

As seen in Fig. 1, the GT Mercury 50 is an open-cycle power plant incorporating a recuperator before the combustion chamber. The recuperator preheats the air using thermal energy from the flue gases exiting the expander. The net power output of the plant is 4.5 MW and its energy efficiency is 37.9%.

The GT systems GE10-1 and Mars100 are coupled with Rankine cycles to form combined-cycle power plants (Fig. 2). In these cases, the flue gas exits the expander with a relatively elevated temperature and it is sent to a HRSG. In this work, the HRSG generates steam at 80 bar and live temperature close to 500 °C. The exact temperature of the steam in each plant depends on the outlet temperature of each incorporated GT system. In all of the cases the temperature difference between the

incoming flue gas and the outgoing superheated steam in the HRSG is kept constant and equal to 20 °C. The generated steam is expanded in the steam turbine of the plants down to 0.05 bar (operational pressure of the condenser).

The net power output of the two combined-cycle power plants is 15 MW. 67% of this power is generated in the GT systems. The energy efficiency of the combined-cycle power plant including the GE-10-1 turbine is 47.0%, while that of the plant including the Mars100 turbine is 45.9%. Thermodynamic data at the stream level can be found in Table A1 of the Appendix.

The above simulations constitute the *base power plants* or *base simulations*. Each of those plants is then coupled with a solar plant to form a hybrid structure. The flow diagrams of the hybrid plants are the same as those of the base cases (Fig. 2), with only change the addition of the solar receiver between the compressor and the combustion chamber of the plants (Fig. 3). The solar plants include a volumetric solar receiver and heliostats, the number of which can vary based on the required load in each plant.

The goal of the solar plants is to increase the inlet temperature of the air before the combustion chamber, in order to decrease the fuel quantity in the GT system and thus increase the overall efficiency of the plant. Once the air passes through the compressor of the GT, its pressure and temperature are increased. The temperature of the air is then further increased to 800 °C or 1000 °C (depending on the requirements of the simulation) passing through the pressurized air receiver of the solar plant. In this work, it is assumed that the total amount of the compressed air passes through the solar receiver. The heated air is then sent to the combustion chamber of the GT system. There, the fuel required to reach the base inlet temperature of the expander of each GT system is added. Together with the inlet temperature of the expander of the GT systems, the net power output of the plants is also kept constant and equal to those of the base simulations. This ensures that material and operational limitations of the already existing GT are not violated.

A pressurized air receiver is modelled to increase the temperature of the air coming from the compressor. This kind of receivers can be either volumetric, made of porous structures, where the radiation is concentrated (the pressurized air passes through the porous media increasing its temperature) [9], or they can consist of pressurized tubes (e.g., the receiver designed in the project SOLUGAS [8]). To the authors' knowledge the efficiency of these receivers range between 0.68 and 0.92 [8,22,23].

The solar radiation is concentrated on the receiver by a heliostat field. For this kind of receiver, the typical configuration of the solar field is elliptically oriented [8]. This configuration has been adopted here as well. Determining the optimal layout is essential from an economic point of view, since the solar field has the highest investment cost in a CSP plant and will thus have a significant impact on the production costs [24]. The optical efficiency of the heliostats depends on the optical properties of the mirrors (i.e., reflectivity), the solar incidence angle between the sunrays and the heliostats, the shading, and the blocking and attenuation factors [25]. The further a heliostat is

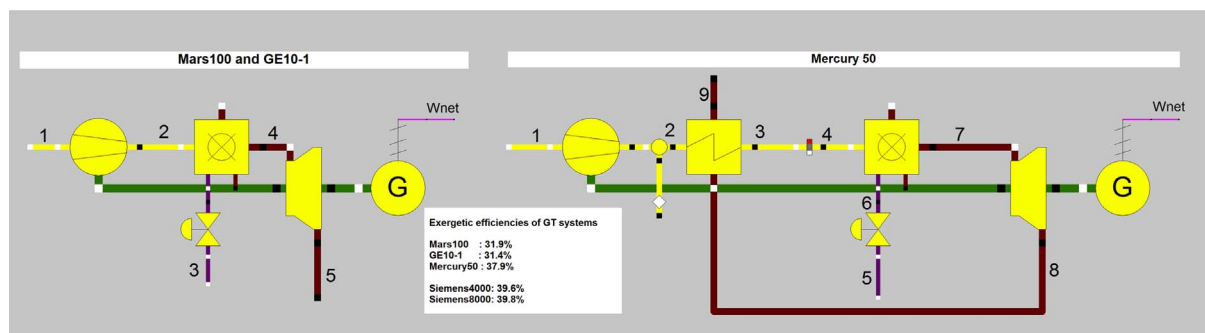


Fig. 1. Flow diagrams of gas turbine systems.

Table 1
Stream data of small-scale gas turbine systems (base simulations).

Stream	Mercury 50			GE10-1			Mars100		
	Mass [kg/s]	Temperature [K]	Pressure [bar]	Mass [kg/s]	Temperature [K]	Pressure [bar]	Mass [kg/s]	Temperature [K]	Pressure [bar]
1	17.7	288.2	1.01	44.0	288.2	1.01	42.5	288.2	1.01
2	17.7	577.8	9.45	44.0	672.1	15.22	42.5	690.5	17.50
3	17.6	833.2	9.09	0.8	288.2	50.00	0.7	288.2	50.00
4	17.6	833.2	9.09	44.8	1324.4	15.02	43.2	1338.5	17.23
5	0.2	288.2	50.00	44.8	757.6	1.03	43.2	761.8	1.03
6	0.2	288.2	9.09						
7	17.8	1359.6	8.81						
8	17.8	888.4	1.01						
9	17.8	647.8	1.01						

Table 2
Operational input parameters of small-scale power plants.

Component	Mercury 50	GE10-1	Mars100
Compressor			
Isentropic efficiency [%]	87.0	85.0	87.0
Mechanical efficiency [%]	98.0	98.0	98.0
Inlet pressure [bar]	1.013	1.013	1.013
Outlet pressure [bar]	9.45	15.22	17.50
Expander			
Isentropic efficiency [%]	88.0	89.4	87.0
Mechanical efficiency [%]	98.0	98.0	98.0
Inlet pressure [bar]	8.814	15.020	17.227
Outlet pressure [bar]	1.013	1.033	1.033
Steam turbine			
Isentropic efficiency [%]	–	95.0	95.0
Mechanical efficiency [%]	–	99.0	99.0
Inlet temperature [°C]	–	464	468
Inlet high pressure [bar]	–	80.0	80.0
Outlet low pressure [bar]	–	0.05	0.05
Pump			
Isentropic efficiency [%]	–	98.0	98.0
Mechanical efficiency [%]	–	98.0	98.0
Generators			
Electrical efficiency [%]	–	98.5	98.5
Motors			
Electrical efficiency [%]	–	87.2	87.2
Heat recovery steam generator			
<i>Evaporator</i>			
Approach temperature [°C]	–	6	6
Pinch point [°C]	–	10	10
<i>Superheater</i>			
ΔT _{min} [°C]	–	20	20

located from the receiver, the more important the losses due to atmospheric attenuation and spillage will be (see Eq. (1)). Thus, for large systems a single oriented field can reduce the optical efficiency significantly [22].

The solar field efficiency is typically calculated as the hourly performance on a few representative days with clear-sky conditions [26,27]. The nominal solar field efficiency varies depending on the solar field layout: 0.7 for a circular field and 0.8 for an oriented field. The annual efficiency decreases slightly due to the daily and seasonal movement of the earth. For example, for a north-field the annual mean field efficiency is around 65% [28]. Schmitz et al. [22] proposed a design of a multiple oriented solar field that could improve the annual solar field efficiency.

In the present study the simulation software SolarPILOT [29] developed by the National Renewable Energy Laboratory (NREL) is used to reproduce all mechanisms of the CSP. The following assumptions are made:

Environment: Cloudless year, visual range 40 km, limb-darkened sun model and flat land.

Heliostat: 10 × 10 m, 8 facet columns, ideally focused, mirror reflectivity: 0.95, soiling factor: 0.95, reflective surface ratio: 0.97, shading factor: 1 and availability: 100%.

Tower: two different tower heights of 80 and 200 m were simulated for low and high thermal energy, respectively. For the simulations where the heat absorbed by the air through the solar receiver is bigger than 100 MW_{th}, multiple receivers are simulated.

Receiver: a volumetric receiver with a secondary concentrator is simulated with a planar receiver reducing the acceptance angle to 30°. The dimensions (width x height) of the receiver are 10 × 10 m. The thermal efficiency of the receiver is η = 76.14% (for air outlet temperature 800 °C) or η = 68% (for air outlet temperature 1000 °C) [23]. The receiver tilting angle is set to 30°.

The design point is the solar noon of the summer solstice (21st of June).

Design characteristics and calculated efficiencies for the solar fields of all plants studied in this paper are shown in Table 3. The results presented in this table are obtained using SolarPILOT, developed by the NREL [29].

Once the optimized heliostat field layout is generated, the optical performance of every heliostat is calculated as:

$$\eta_{hel} = \cos\theta \cdot \eta_{ref} \cdot \eta_s \cdot \eta_{bl} \cdot \eta_{int} \cdot \eta_{at} \quad (1)$$

where, cosθ is the angle between the heliostat normal and the solar radiation direction.

The reflection efficiency, η_{ref}, is calculated as the product of the soiling factor and the mirror reflectance. The shading factor (or shading efficiency, η_s) is considered constant and equal to one. The blocking factor (η_{bl}) is calculated using the vector clipping method [30]. The 2D Gauss-Hermite quadrature method is used to evaluate the intercept factor (η_{int}) for individual heliostats. This analytical approach is incorporated into SolarPILOT [30]. Details on this numerical integration method can be found in [31].

The attenuation factor can be calculated as:

$$\eta_{at}(r) = 0.006789 + 0.10463 \cdot r - 0.017 \cdot r^2 + 0.002845 \cdot r^3 \quad (2)$$

Finally, the field performance can be calculated as:

$$\eta_{field} = \frac{\sum_{i=1}^N \eta_{hel}}{N} \quad (3)$$

The combined efficiency of the total solar system (η_{sol}) is calculated as: η_{sol} = η_{field}η_{receiver}. Potential practical technological challenges associated with the construction and operation of the examined systems are not studied.

Thermodynamic data at the stream-level of the hybrid plants can be found in Tables A2 and A3 of the Appendix.

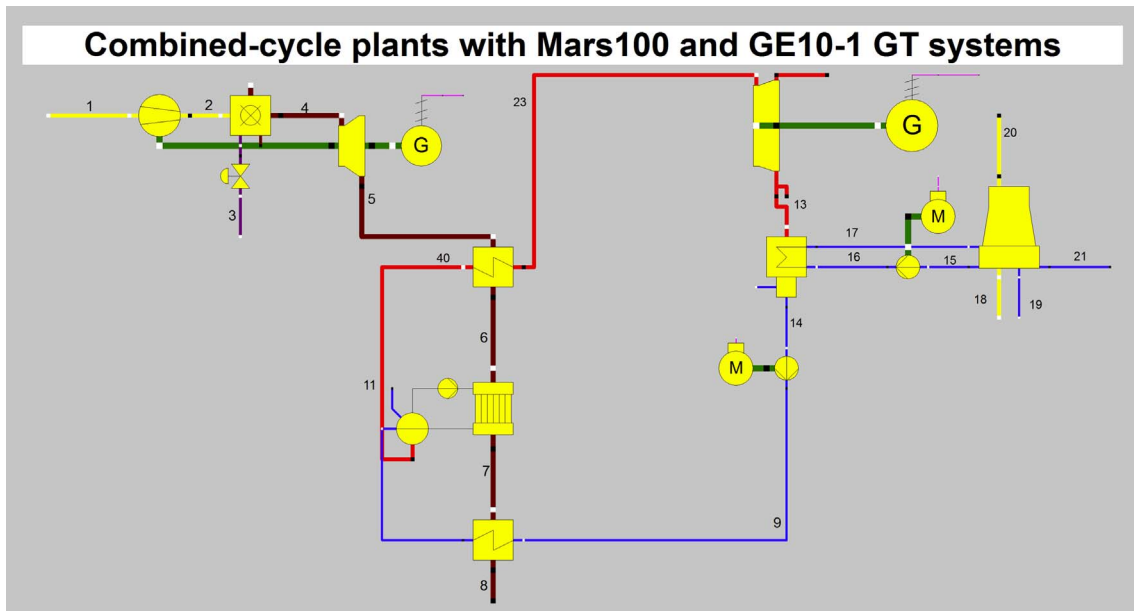
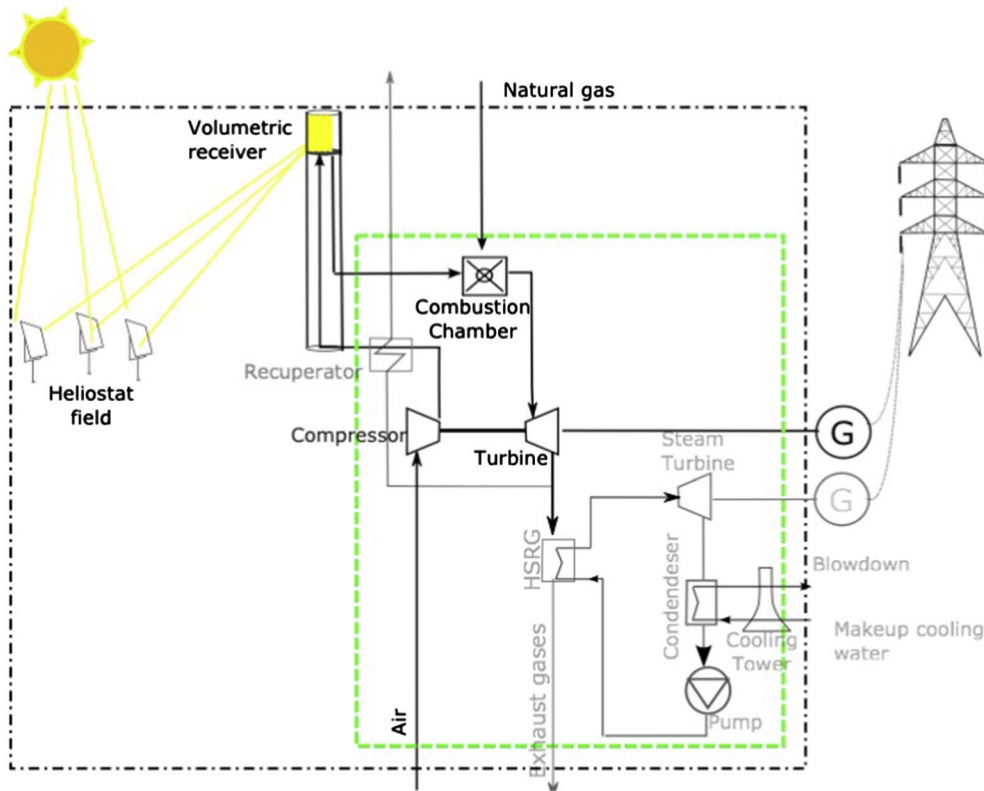


Fig. 2. Flow diagrams of combined-cycle power plants.

Fig. 3. General flow diagram of hybrid systems.



3. Methods

The evaluation of the overall power plants is realized using both exergy and energy efficiencies, while the component-level assessment is realized with exergy analysis. The definitions of exergy rates of fuel and product for the individual components of the plants are shown in Table 4.

The exergy destruction of component k is defined as the difference between its exergy rates of fuel and product: $\dot{E}_{D,k} = \dot{E}_{F,k} - \dot{E}_{P,k}$. The calculation of the exergy destruction of the overall plant (tot) involves its total exergy losses: $\dot{E}_{D,tot} = \dot{E}_{F,tot} - \dot{E}_{P,tot} - \dot{E}_{L,tot}$.

The exergy efficiency at the component level is defined as the ratio between the corresponding exergy rates of product and fuel: $\epsilon_k = \frac{\dot{E}_{P,k}}{\dot{E}_{F,k}}$. In this work, the efficiency of the overall plant is defined in two ways, based on the thermodynamic boundaries depicted in Fig. 3. The first definition (Eq. (4)) does not include the efficiency of the conversion of solar radiation into thermal energy, while the second definition (Eq. (5)) includes it (ϵ_{sol} : exergy efficiency of the solar receiver):

$$\epsilon_{tot,excl,sol} = \frac{\dot{E}_{P,tot}}{\dot{E}_{F,tot}} = \frac{\dot{W}_{GT} + \dot{W}_{ST} - \dot{W}_{comp} - \dot{W}_{pump}}{(\dot{m}_{NG} \cdot e_{NG}) + [\dot{m}_{air} \cdot (e_{air,2} - e_{air,1})]} \quad (4)$$

Table 3
Design characteristics and calculated efficiencies of solar plant.

Outlet temperature of solar receiver	Mercury 50		Mars 100		GE 10-1		SGT5-4000F		SGT5-8000H	
	800 °C	1000 °C	800 °C	1000 °C	800 °C	1000 °C	800 °C	1000 °C	800 °C	1000 °C
No. of receivers [–]	1	1	1	1	1	1	1	3	3	5
No. of heliostats [–]	207	338	372	666	360	653	5166	8000	5619	9365
Solar field optical efficiency [%]	76.1	73.3	72.6	68.5	72.9	68.7	67.3	68.0	66.5	66.5
Optical efficiency incl. receiver [%]	71.5	68.9	68.2	64.4	68.5	64.6	63.2	63.9	62.6	62.6
Receiver thermal efficiency [%]	76.1	68.0	76.1	68.0	76.1	68.0	76.1	68.0	76.1	68.0
Overall solar energy efficiency [%]	57.9	49.8	55.2	46.6	55.5	46.7	51.2	46.2	50.6	45.2
Overall solar exergy efficiency [%]	43.3	38.7	39.7	35.0	39.6	34.9	37.2	35.0	36.7	34.2

Table 4
Definitions of exergy of the fuel and product for the examined power plants (based on Fig. 2).

Component k	$\dot{E}_{F,k}$	$\dot{E}_{P,k}$
Compressor	\dot{W}_{comp}	$\dot{E}_2 - \dot{E}_1$
Combustion chamber	\dot{E}_3	$\dot{E}_4 - \dot{E}_2$
Expander	$\dot{E}_4 - \dot{E}_5$	\dot{W}_{exp}
Steam turbine	$\dot{E}_{23} - \dot{E}_{13}$	\dot{W}_{ST}
Economizer	$\dot{E}_7 - \dot{E}_8$	$\dot{E}_{10} - \dot{E}_9$
Evaporator	$\dot{E}_6 - \dot{E}_7$	$\dot{E}_{11} - \dot{E}_{10}$
Superheater	$\dot{E}_5 - \dot{E}_6$	$\dot{E}_{23} - \dot{E}_{40}$
Pump	\dot{W}_{pump}	$\dot{E}_9 - \dot{E}_{14}$

$$\epsilon_{tot, inclsol} = \frac{\dot{E}_{P,tot}}{\dot{E}_{F,tot}} = \frac{\dot{W}_{GT} + \dot{W}_{ST} - \dot{W}_{comp} - \dot{W}_{pump}}{(\dot{m}_{NG} \cdot e_{NG}) + [(\dot{m}_{air} \cdot (e_{air,2} - e_{air,1})) / \epsilon_{sol}]} \quad (5)$$

where e and \dot{m} are the specific exergy and mass flow rates of material streams, respectively, ϵ is the exergy efficiency and \dot{W} is the power output. The numerator of Eqs. (4) and (5) represents the total net power output generated in each plant, calculated subtracting from the power generated in the GT system and the steam turbine (ST), the required power by the compressor (comp) and the pumps (pump). The denominator includes the exergy input of fuel (natural gas, NG) and air, subtracting the increase in exergy of the air exiting the compressor ($e_{air,1}$) and entering the combustion chamber ($e_{air,2}$), achieved with the solar plant.

It is apparent that Eq. (5) depends on the exergy efficiency of the solar plant. Higher energy and exergy efficiencies of conversion of the solar irradiation into useful thermal energy lead to higher overall plant efficiencies.

The exergy efficiency of the solar plant (ϵ_{sol}) is defined as follows:

$$\epsilon_{sol} = \frac{\dot{E}_{P,sol}}{\dot{E}_{F,sol}} = \frac{\dot{E}_{P,sol}}{\dot{Q}_{sol,rad} \cdot \Psi} = \frac{\dot{E}_{P,sol}}{\dot{Q}_{sol,abs}} \frac{n_{sol}}{\Psi} \quad (6)$$

where $\dot{E}_{P,sol}$ is the exergy of the solar energy absorbed by the air stream heated and $\dot{E}_{F,sol}$ is the exergy of the solar energy irradiated from the sun. The exergy of the solar irradiation is calculated based on the total energy available from the sun. The ratio Ψ between exergy and energy is defined as follows [32]:

$$\Psi = 1 - \frac{4}{3} \frac{T_a}{T_s} + \frac{1}{3} \left(\frac{T_a}{T_s} \right)^4 \text{ with } T_a \text{ the ambient temperature and } T_s \text{ the apparent black body temperature equal to 5600 K.}$$

Analogous to the exergy efficiencies, the energy efficiencies of the plants are calculated using Eqs. (7) and (8):

$$\eta_{tot, exclsol} = \frac{\dot{Q}_{P,tot}}{\dot{Q}_{F,tot}} = \frac{\dot{W}_{GT} + \dot{W}_{ST} - \dot{W}_{comp} - \dot{W}_{pump}}{(\dot{m}_{NG} \cdot h_{NG}) + [\dot{m}_{air} \cdot (h_{air,2} - h_{air,1})]} \quad (7)$$

$$\eta_{tot, inclsol} = \frac{\dot{Q}_{P,tot}}{\dot{Q}_{F,tot}} = \frac{\dot{W}_{GT} + \dot{W}_{ST} - \dot{W}_{comp} - \dot{W}_{pump}}{(\dot{m}_{NG} \cdot h_{NG}) + [(\dot{m}_{air} \cdot (h_{air,2} - h_{air,1})) / \eta_{sol}]} \quad (8)$$

4. Results and discussion

The component-level results of the exergy analysis for the simulations of the small-scale power plants (base and hybrid simulations) are presented in Tables 5–7. Table 5 shows the results of the base simulations. Tables 6 and 7 present the results of the hybrid plants, for combustion inlet air temperatures of 800 °C and 1000 °C, respectively. Stream-level data can be found in Tables A1–A3 of the Appendix. The inlet temperature of the expander of the GT systems is in all cases equal to that of the base case, since we study the effect of the addition of solar receivers to chosen existing GTs. Thus, future technological progress of GT systems is not accounted for here.

As seen, the base case of the Mercury 50 power gas-turbine plant has an exergy efficiency of 36.3%, while the two combined cycles including the turbines Mars100 and GE10-1 achieve significantly higher efficiencies (44.7% and 45.1%). This shows the importance of the addition of the bottoming cycle in the two combined-cycle plants that largely increases the efficiency of individual GT systems (in the order of 35%). Comparing the two combined cycles, we see that the plant with GE10-1 results in a higher overall efficiency, mainly due to the higher efficiency of the GT system itself.

The incorporation of the solar plants to increase the inlet temperature of the combustor of the GT systems to 800 °C, results in an increase in the overall exergy efficiencies of the plants, when the efficiency definition of Eq. (4) is used. The increase is in the order of 6 percentage points (pp) for Mercury 50, while it reaches 10 and 11 pp for the combined cycles of Mars100 and GE10-1, respectively. These results are primarily driven by the significantly reduced mass flow of fuel required to reach the constant inlet temperature of the expander, when compared to the base case. In addition, the efficiency of the combustion process is significantly increased due to the increased inlet temperature of the combustion air.

Calculating the operational exergy efficiencies of the plants using Eq. (5), on the other hand, leads to different conclusions. In this case, the efficiency is affected by the efficiency of the conversion of solar radiation. This means that the higher the solar input, the higher the associated efficiency penalty will be. Accounting for the conversion efficiency approximately doubles the total exergy of the fuel of the plants, when compared to that used in Eq. (4). This leads to significantly decreased overall exergy efficiencies of the plants in comparison to their base operation. This efficiency reduction is in the order of 6 pp in the Mercury 50 GT system and in the order of 12 pp in the combined cycles (see Table 6). In addition, with Eq. (5) the difference between the efficiencies of GE10-1 and Mars100 decreases significantly, with the GE10-1 performing only slightly better than the Mars100.

Table 5
Component-level results of the exergy analysis for the small-scale power plants (base simulations).

Mars100					PGT10					Mercury 50							
Component k	$\dot{E}_{F,k}$	$\dot{E}_{P,k}$	$\dot{E}_{D,k}$	ϵ_k	\dot{E}_L	Component k	$\dot{E}_{F,k}$	$\dot{E}_{P,k}$	$\dot{E}_{D,k}$	ϵ_k	\dot{E}_L	Component k	$\dot{E}_{F,k}$	$\dot{E}_{P,k}$	$\dot{E}_{D,k}$	ϵ_k	\dot{E}_L
Compressor	16.69	15.44	1.25	92.5		Compressor	16.18	14.80	1.38	91.5		Compressor	5.35	4.90	0.46	91.5	
Combustion chamber	33.58	22.71	10.87	67.6		Combustion chamber	34.24	23.00	11.24	67.2		Combustion chamber	12.47	8.61	3.86	69.1	
Expander	29.36	27.14	2.22	92.4		Expander	28.97	27.11	1.86	93.6		Expander	10.63	9.96	0.67	93.7	
Solar plant	–	–	–	–		Solar plant	–	–	–	–		Solar plant	–	–	–	–	
Superheater	1.40	1.22	0.18	87.2		Superheater	1.36	1.19	0.18	87.2		Recuperator	3.15	2.80	0.35	88.8	
Evaporator	3.20	2.85	0.35	89.1		Evaporator	3.19	2.84	0.34	89.2							
Economizer	2.09	1.50	0.60	71.5		Economizer	2.09	1.49	0.60	71.3							
Steam turbine	5.15	4.86	0.29	94.3		Steam turbine	5.11	4.82	0.29	94.3							
Condenser	0.45	–	0.34	–		Condenser	0.45	–	0.33	–							
Pump	0.04	0.03	0.00	90.3		Pump	0.04	0.03	0.00	90.3							
Cooling tower	1.00	–	0.04	–		Cooling tower	1.00	–	0.04	–							
Ex.Eff Eq. (4)	33.64	15.03	16.37	44.7	2.24	Ex.Eff Eq. (4)	34.30	15.47	16.52	45.1	2.31	Ex.Eff Eq. (4)	12.50	4.54	5.43	36.3	2.52
Ex.Eff Eq. (5)	n/a	n/a	n/a	n/a		Ex.Eff Eq. (5)	n/a	n/a	n/a	n/a		Ex.Eff Eq. (5)	n/a	n/a	n/a	n/a	
En.Eff Eq. (7)				46.6		En.Eff Eq. (7)				47.0		En.Eff Eq. (7)				37.9	
En.Eff Eq. (8)	n/a	n/a	n/a	n/a		En.Eff Eq. (8)	n/a	n/a	n/a	n/a		En.Eff Eq. (8)	n/a	n/a	n/a	n/a	

Table 6
Component-level results of the exergy analysis for the small-scale hybrid power plants (inlet temperature of the combustion chamber: 800 °C).

Mars100					PGT10					Mercury 50							
Component k	$\dot{E}_{F,k}$	$\dot{E}_{P,k}$	$\dot{E}_{D,k}$	ϵ_k	\dot{E}_L	Component k	$\dot{E}_{F,k}$	$\dot{E}_{P,k}$	$\dot{E}_{D,k}$	ϵ_k	\dot{E}_L	Component k	$\dot{E}_{F,k}$	$\dot{E}_{P,k}$	$\dot{E}_{D,k}$	ϵ_k	\dot{E}_L
Compressor	17.77	16.44	1.33	92.5		Compressor	17.23	15.75	1.47	91.5		Compressor	5.35	4.90	0.46	91.5	
Combustion chamber	15.38	10.78	4.60	70.1		Combustion chamber	14.83	10.36	4.47	69.9		Combustion chamber	7.01	4.90	2.10	70.0	
Expander	30.59	28.26	2.33	92.4		Expander	30.18	28.22	1.95	93.5		Expander	10.50	9.83	0.66	93.7	
Solar plant	70.53	11.99	58.54	17.0		Solar plant	35.57	12.69	22.87	35.7		Solar plant	7.72	3.34	4.38	43.3	
Superheater	33.39	11.99	21.40	35.9		Superheater	1.31	1.14	0.17	87.1		Recuperator	3.13	2.80	0.33	89.3	
Evaporator	3.19	2.85	0.34	89.3		Evaporator	3.17	2.84	0.34	89.4							
Economizer	2.10	1.49	0.61	71.1		Economizer	2.10	1.49	0.61	70.9							
Steam turbine	5.10	4.81	0.29	94.3		Steam turbine	5.06	4.77	0.29	94.3							
Condenser	0.45	–	0.33	–		Condenser	0.45	–	0.33	–							
Pump	0.04	0.03	0.00	90.3		Pump	0.04	0.03	0.00	90.3							
Cooling tower	1.00	–	0.04	–		Cooling tower	1.00	–	0.04	–							
Ex.Eff Eq. (4)	27.43	15.03	10.29	54.8	2.12	Ex.Eff Eq. (4)	27.59	15.49	9.92	56.1	2.18	Ex.Eff Eq. (4)	10.38	4.41	3.65	42.5	2.32
Ex.Eff Eq. (5)	45.65	15.03	28.50	32.9		Ex.Eff Eq. (5)	46.94	15.49	31.45	33.0		Ex.Eff Eq. (5)	14.75	4.41	10.34	29.9	
En.Eff Eq. (7)				45.9		En.Eff Eq. (7)				46.4		En.Eff Eq. (7)				38.2	
En.Eff Eq. (8)				31.8		En.Eff Eq. (8)				31.8		En.Eff Eq. (8)				29.3	

Table 7
Component-level results of the exergy analysis for the small-scale hybrid power plants (inlet temperature of the combustion chamber: 1000 °C).

Mars100					PGT10					Mercury 50							
Component k	$\dot{E}_{F,k}$	$\dot{E}_{P,k}$	$\dot{E}_{D,k}$	ϵ_k	\dot{E}_L	Component k	$\dot{E}_{F,k}$	$\dot{E}_{P,k}$	$\dot{E}_{D,k}$	ϵ_k	\dot{E}_L	Component k	$\dot{E}_{F,k}$	$\dot{E}_{P,k}$	$\dot{E}_{D,k}$	ϵ_k	\dot{E}_L
Compressor	18.39	17.02	1.38	92.5		Compressor	17.83	16.31	1.52	91.5		Compressor	5.35	4.90	0.46	91.5	
Combustion chamber	4.40	2.80	1.60	63.6		Combustion chamber	3.63	2.23	1.40	61.4		Combustion chamber	2.31	1.50	0.81	64.9	
Expander	31.29	28.90	2.39	92.3		Expander	30.87	28.86	2.01	93.5		Expander	10.38	9.72	0.66	93.7	
Solar plant	53.53	20.09	33.44	37.5		Solar plant	56.11	20.95	35.16	37.3		Solar plant	16.71	6.46	10.24	38.7	
Superheater	1.32	1.15	0.17	87.1		Superheater	1.29	1.12	0.17	87.0		Recuperator	3.11	2.80	0.32	89.8	
Evaporator	3.19	2.85	0.34	89.4		Evaporator	3.17	2.84	0.33	89.5							
Economizer	2.11	1.49	0.61	71.0		Economizer	2.10	1.49	0.61	70.8							
Steam turbine	5.08	4.79	0.29	94.3		Steam turbine	5.03	4.75	0.29	94.3							
Condenser	0.45	–	0.33	–		Condenser	0.44	–	0.33	–							
Pump	0.04	0.03	0.00	90.3		Pump	0.04	0.03	0.00	90.3							
Cooling tower	1.00	–	0.04	–		Cooling tower	1.00	–	0.04	–							
Ex.Eff Eq. (4)	24.55	15.03	7.40	61.2	2.13	Ex.Eff Eq. (4)	24.65	15.50	6.95	62.9	2.20	Ex.Eff Eq. (4)	8.80	4.30	2.33	48.9	2.16
Ex.Eff Eq. (5)	61.92	15.03	46.90	24.3		Ex.Eff Eq. (5)	63.76	15.50	48.26	24.3		Ex.Eff Eq. (5)	19.04	4.30	14.74	22.6	
En.Eff Eq. (7)				45.5		En.Eff Eq. (7)				46.0		En.Eff Eq. (7)				38.5	
En.Eff Eq. (8)				22.8		En.Eff Eq. (8)				22.8		En.Eff Eq. (8)				21.3	

Table 8
Result comparison of the two definitions of the energy and exergy efficiencies.

	Energy efficiency		Exergy efficiency	
	Eq. (1)	Eq. (2)	Eq. (1)	Eq. (2)
GT-10				
Base	46.98	–	45.10	–
800	46.38	31.78	56.14	33.00
1000	46.04	22.77	62.88	24.31
Mars100				
Base	46.55	–	44.69	–
800	45.89	31.78	54.79	32.93
1000	45.52	22.76	61.21	24.27
Mercury 50				
Base	37.87	–	36.35	–
800	38.20	29.33	42.52	29.91
1000	38.51	21.31	48.89	22.59

Although the GE10-1 requires a larger input of thermal energy (i.e., larger amount of solar radiation) to compensate for the relatively lower output temperature of the compressor, it is characterized by a marginal increase in solar plant efficiency.

When increasing the inlet temperature of the combustion chamber to 1000 °C (Table 7), the exergy efficiencies of the combustion chambers of the hybrid plants decrease in comparison to the previous case of 800 °C. Although the mass flow of natural gas decreases further due to the increased inlet temperature of the combustion chamber, the mass flow of the air increases significantly in order to keep the temperature of the expander constant (increased air-to-fuel ratio). It is seen that the efficiency of the combustion chamber is maximized for an inlet air temperature between 800 °C and 1000 °C. Nevertheless, although the individual exergy efficiencies of the combustion chambers decrease, the total efficiencies of the plants, calculated using Eq. (4), continue to increase notably (between 6.4 and 6.7 pp). This is due to the important decrease in the exergy of the fuel of the plant substituted by the thermal energy contribution of the solar plants. On the other hand, when Eq. (5) is applied, the total exergy of the fuel increases by 2.5 times relative to Eq. (4). In this case, the low efficiency of the solar conversion results in a declining trend in the total efficiencies. The resulting efficiencies are lower than those calculated for combustion air inlet temperature of 800 °C (a difference of 7 pp in the case of Mercury-50 and 8 in the other two plants).

When looking at the energy efficiencies (Eqs. (7) and (8)), the results differ (shown in Tables 5–7). For Mercury 50 the energy efficiency increases by 0.3 pp when the inlet temperature of the combustion chamber is increased to 800 °C and by another 0.3 pp when it is increased further to 1000 °C. This positive effect is due to the recuperator of the plant that limits the negative effect of the solar thermal addition on the denominator of the efficiency. On the other hand, the overall

energy efficiencies of the combined cycle power plants are seen to decrease with increasing inlet temperature of the combustion chamber. Specifically, when increasing the inlet combustion temperature to 800 °C and 1000 °C the overall energy efficiency of Eq. (8) decreases by approximately 0.6 and 1 pp relative to the base case. Thus, the energy efficiency shows that higher temperatures at the inlet of the combustion chamber do not improve the overall performance of the plant. This result contradicts the results obtained using the exergy analysis and is an indicator of the importance of exergy-based methods in the analysis and evaluation of energy conversion systems.

The described analyses and evaluation was realized in the design phase of the plants. As mentioned, the total power output of the combined-cycle power plants was kept constant and equal that of the base simulations. Thus, a slight increase in the power output of the GT system due to the temperature increase from the solar receivers leads to a small decrease in the power output of the steam turbine. Although the mass flow of the fuel decreases with increasing input of the solar receiver, the mass flow of the air (air-to-fuel ratio) increases to keep the temperature inlet of the expander constant. Overall, in the hybrid plants we obtain larger flue gas mass flows, when compared to the base cases. This leads to a decreased outlet temperature of the GT system that consequently results in a somewhat increased temperature of exhaust gases (the temperature differences in the HRSG are kept constant). The exergy and energy efficiencies of the small-scale plants in the different temperature scenarios are presented in Table 8.

The above evaluated small-scale power plants had approximate capacities of 4–15 MW. In order to realize a more complete evaluation of the solar technology studied, we also evaluate two large-scale scenarios. These include two combined-cycle power plants incorporating the large-scale GT systems Siemens SGT5-4000F and SGT5-8000H. The base simulations of these systems are based on the GT library of the software EbsilonProfessional. Thermodynamic and operational data used in the base simulations of the individual components of the GT systems can be seen in Tables 9 and 10. The stream-level data of the combined-cycle power plants that incorporate the two large-scale turbines can be found in Table A6 of the Appendix of the paper. The results of the exergy analysis at the component level of the base simulations of the two plants and their simulations incorporating the solar plants are presented in Tables 11–13.

In an analogous manner to the small-scale plants, the energy efficiencies of the plants decrease with increasing inlet temperature of the combustion chamber. The exergy efficiencies of the plants (using Eq. (4)), on the other hand, increase significantly. The power plant with the largest GT system (SGT5-8000H) results in the highest overall exergy efficiency. When looking at the exergy efficiencies of the individual components, that of the combustion chamber in SGT5-8000H continues to increase with increasing contribution of the solar receiver. On the other hand, in the case of SGT5-4000F, the efficiency of the combustion chamber slightly decreases between the scenarios of inlet combustor temperatures 800 and 1000 °C. As in the small-scale plants, in SGT5-4000F the increasing mass flow of air starts to cause a

Table 9
Stream data of large-scale gas turbine systems (base simulations).

Stream	SGT5-4000F			SGT5-8000H		
	Mass [kg/s]	Temperature [K]	Pressure [bar]	Mass [kg/s]	Temperature [K]	Pressure [bar]
1	706.6	288.2	1.01	855.6	288.2	1.01
2	706.6	721.6	19.04	855.6	721.6	19.50
3	15.4	288.2	50.00	20.2	288.2	50.00
4	722.0	1547.6	18.77	875.8	1608.5	19.23
5	722.0	850.4	1.03	875.8	890.7	1.03

Table 10
Operational input parameters of large-scale power plants (when different than those shown in Table 2).

Component	SGT5-4000F	SGT5-8000H
<i>Compressor</i>		
Isentropic efficiency [%]	84.0	85.0
Outlet pressure [bar]	19.04	19.50
<i>Expander</i>		
Isentropic efficiency [%]	91.0	90.3
Inlet pressure [bar]	18.77	19.23
Outlet pressure [bar]	1.033	1.033
<i>Steam turbine</i>		
Inlet temperature [K]	830	869

reduction in the efficiency of the combustion chamber for an inlet temperature somewhat lower than 1000 °C.

From the above we see that the addition of a solar plant has a positive effect on the operation of the combustion chambers of GT plants up to a specific temperature. This temperature limit depends on the size

Table 11
Component-level results of the exergy analysis for the large-scale power plants (base simulations).

Siemens SGT5-4000F						Siemens SGT5-8000H					
Component k	$\dot{E}_{F,k}$	$\dot{E}_{P,k}$	$\dot{E}_{D,k}$	ϵ_k	\dot{E}_L	Component k	$\dot{E}_{F,k}$	$\dot{E}_{P,k}$	$\dot{E}_{D,k}$	ϵ_k	\dot{E}_L
Compressor	328.66	300.61	28.05	91.5		Compressor	369.79	339.81	29.97	91.9	
Combustion chamber	810.51	572.19	238.32	70.6		Combustion chamber	989.37	704.92	284.45	71.2	
Expander	658.01	623.13	34.88	94.7		Expander	773.89	731.88	42.01	94.6	
Solar plant	1.00	0.00	1.00	50.0		Solar plant	1.00	0.00	1.00	50.0	
Superheater	50.97	44.62	6.36	87.5		Superheater	73.01	63.96	9.04	87.6	
Evaporator	82.64	71.89	10.75	87.0		Evaporator	104.52	90.10	14.42	86.2	
Economizer	50.03	37.72	12.31	75.4		Economizer	61.20	47.27	13.93	77.2	
Steam turbine	143.20	135.07	8.13	94.3		Steam turbine	187.23	176.60	10.62	94.3	
Condenser	11.91	–	8.85	–		Condenser	15.20	–	11.30	–	
Pump	0.97	0.88	0.09	90.3		Pump	1.21	1.10	0.12	90.3	
Cooling tower	1.00	–	1.14	–		Cooling tower	1.00	–	1.45	–	
Ex.Eff Eq. (4)	811.62	421.98	355.47	52.0	34.17	Ex.Eff Eq. (4)	990.62	529.23	425.58	53.4	35.81
Ex.Eff Eq. (5)	n/a	n/a	n/a	n/a		Ex.Eff Eq. (5)	n/a	n/a	n/a	n/a	
En.Eff Eq. (7)				54.1		En.Eff Eq. (7)				55.6	
En.Eff Eq. (8)	n/a	n/a	n/a	n/a		En.Eff Eq. (8)	n/a	n/a	n/a	n/a	

Table 12
Component-level results of the exergy analysis for the large-scale hybrid power plants (inlet temperature of the combustion chamber: 800 °C).

Siemens SGT5-4000F						Siemens SGT5-8000H					
Component k	$\dot{E}_{F,k}$	$\dot{E}_{P,k}$	$\dot{E}_{D,k}$	ϵ_k	\dot{E}_L	Component k	$\dot{E}_{F,k}$	$\dot{E}_{P,k}$	$\dot{E}_{D,k}$	ϵ_k	\dot{E}_L
Compressor	344.68	315.26	29.42	91.5		Compressor	387.20	355.81	31.38	91.9	
Combustion chamber	505.55	369.40	136.15	73.1		Combustion chamber	646.25	476.38	169.86	73.7	
Expander	676.17	640.07	36.10	94.7		Expander	793.92	750.51	43.41	94.5	
Solar plant	552.48	200.33	352.15	36.3		Solar plant	620.78	225.09	395.69	36.3	
Superheater	49.32	43.16	6.17	87.5		Superheater	70.86	62.07	8.79	87.6	
Evaporator	82.17	71.63	10.55	87.2		Evaporator	104.04	89.85	14.19	86.4	
Economizer	50.11	37.58	12.53	75.0		Economizer	61.38	47.15	14.23	76.8	
Steam turbine	141.42	133.40	8.03	94.3		Steam turbine	185.06	174.56	10.50	94.3	
Condenser	11.82	–	8.79	–		Condenser	15.10	–	11.23	–	
Pump	0.97	0.87	0.09	90.3		Pump	1.21	1.09	0.12	90.3	
Cooling tower	1.00	–	1.13	–		Cooling tower	1.00	–	1.44	–	
Ex.Eff Eq. (4)	707.04	421.25	255.52	59.6	30.27	Ex.Eff Eq. (4)	872.65	528.42	313.40	60.6	30.83
Ex.Eff Eq. (5)	1045.80	421.25	594.28	40.3		Ex.Eff Eq. (5)	1260.58	528.42	701.33	41.9	
En.Eff Eq. (7)				53.8		En.Eff Eq. (7)				55.3	
En.Eff Eq. (8)				39.5		En.Eff Eq. (8)				41.2	

and the air-to-fuel ratio of the GT system and the inlet temperature of the expander. In the five cases presented in this paper, the increase of the combustion air to 1000 °C had a positive effect in only one large-scale plant of a power output of 530 MW. Nevertheless, it is seen that the effect of the temperature increase on the operation of the combustion chamber does not dictate the effect on the overall plant. Thus, to conclude whether the hybridization with a solar plant is beneficial or not, we must look at the efficiency results of the total plants. Thus, it is necessary to define explicitly the efficiency equation used, in order to allow accurate and transparent comparisons.

5. Conclusions

This article studied the performance impact of the hybridization of solar plants, including a volumetric solar receiver, with five existing gas turbine systems. The aim of incorporating solar power systems was to increase the inlet temperature of the combustion air of the gas turbine systems by heating up the air exiting the compressor using solar energy. Since the study was based on real gas turbine systems, the inlet temperatures of the expanders were kept constant, while the fuel input, and thus the air-to-fuel ratios of the systems, were varied to satisfy the new

Table 13
Component-level results of the exergy analysis for the large-scale hybrid power plants (inlet temperature of the combustion chamber: 1000 °C).

Siemens SGT5-4000F						Siemens SGT5-8000H					
Component k	$\dot{E}_{F,k}$	$\dot{E}_{P,k}$	$\dot{E}_{D,k}$	ϵ_k	\dot{E}_L	Component k	$\dot{E}_{F,k}$	$\dot{E}_{P,k}$	$\dot{E}_{D,k}$	ϵ_k	\dot{E}_L
Compressor	354.96	324.66	30.30	91.5		Compressor	398.38	366.09	32.29	91.9	
Combustion chamber	309.90	225.89	84.02	72.9		Combustion chamber	426.70	315.03	111.68	73.8	
Expander	687.80	650.92	36.89	94.6		Expander	806.76	762.45	44.31	94.5	
Solar plant	907.45	343.29	564.16	37.8		Solar plant	1018.61	385.34	633.27	37.8	
Superheater	48.31	42.26	6.05	87.5		Superheater	69.53	60.89	8.64	87.6	
Evaporator	81.88	71.45	10.42	87.3		Evaporator	103.74	89.70	14.04	86.5	
Economizer	50.15	37.49	12.66	74.8		Economizer	61.48	47.06	14.42	76.5	
Steam turbine	140.32	132.35	7.96	94.3		Steam turbine	183.71	173.28	10.42	94.3	
Condenser	11.76	–	8.74	–		Condenser	15.04	–	11.18	–	
Pump	0.96	0.87	0.09	90.3		Pump	1.21	1.09	0.12	90.3	
Cooling tower	1.00	–	1.12	–		Cooling tower	1.00	–	1.43	–	
Ex.Eff Eq. (4)	654.39	420.78	204.81	64.3	28.80	Ex.Eff Eq. (4)	813.39	527.90	256.77	64.9	28.72
Ex.Eff Eq. (5)	1292.34	420.78	842.76	32.6		Ex.Eff Eq. (5)	1554.33	527.90	997.71	34.0	
En.Eff Eq. (7)				53.5		En.Eff Eq. (7)				55.1	
En.Eff Eq. (8)				31.1		En.Eff Eq. (8)				32.6	

operational conditions.

Three of the cases studied were small-scale power plants, involving an open gas-turbine plant with a recuperator and two combined-cycle power plants. Two large-scale plants were also studied in order to evaluate possibilities for scaling-up the technology. All of the plants were examined using exergy analysis at the component-level, while the overall performance of the structures was evaluated using both energy and exergy efficiencies. The efficiencies were defined in two ways: first, neglecting and, second, including the solar-to-thermal conversion in the solar plants. However, both definitions included the required thermal energy to achieve the aimed temperature increase.

The overall exergy efficiencies of the plants (without including the efficiency of the solar plant) increased significantly with increasing inlet temperature of the combustion chamber (i.e., increasing solar contribution). This was a direct result of the fuel mass flow that decreased with increasing combustor temperature. Since the outlet temperature of the combustion chamber –and inlet temperature of the expander of the gas turbine system– was kept constant, the temperature difference between the inlet and outlet of the combustor decreased as its inlet temperature increased due to the solar receiver. However, it was seen that the individual efficiencies of the combustion chambers in the small-scale plants presented a maximum efficiency for combustion inlet air temperatures between 800 °C and 1000 °C. This maximum shifted towards the higher inlet temperature as the outlet temperature of the combustor increased. This effect was more pronounced in the large-scale plants. On the other hand, it was seen that the significant amount of solar energy required to increase the inlet temperature of the combustion chamber to 800 and 1000 °C caused a relative decrease in

the energy efficiencies of the plants. The only way to achieve increasing energy efficiencies with higher inlet temperatures in the combustor and constant inlet turbine temperature, would be to ignore the solar thermal energy in the equation of the efficiency, by assuming zero cost and thermodynamic penalty of the solar radiation.

When the efficiency of the solar plant (the conversion of solar irradiation into thermal energy) was accounted for in the efficiency calculation, it was seen that the exergy efficiency decreased with increasing solar contribution, i.e., increasing temperature at the inlet temperature of the combustor. This was due to the relatively low efficiencies of the solar plants. This, in combination with the large solar input, affected the overall results significantly. Similar results were obtained when evaluating the hybridization scenarios for existing large-scale combined-cycle power plants. Nevertheless, in this case, the impact of including solar energy was relatively weaker than in the small-scale plants.

Acknowledgments

The authors would like to thank the University Carlos III of Madrid, the European Union's Seventh Framework Programme for research, technological development and demonstration, the Ministerio de Economía y Competitividad, Ministerio de Educación, Cultura y Deporte (CEI-15-17) and Banco Santander for the financial support of the projects COFUND2014-51509 (CONEX-OPTIHYP, grant agreement no 600371), ENE2014-54942-R and ENE2015-69486-R (MINECO / FEDER, UE).

Appendix

See Tables A1–A6.

Table A1
Stream data of small-scale combined-cycle power plants (base simulations).

Stream	Mars100				GE10-1			
	Mass [kg/s]	Temperature [K]	Pressure [bar]	Exergy [MW]	Mass [kg/s]	Temperature [K]	Pressure [bar]	Exergy [MW]
1	39.18	288.15	1.01	0.061	39.90	288.15	1.01	0.062
2	39.18	690.54	17.50	15.498	39.90	672.07	15.22	14.859
3	0.64	288.15	50.00	33.582	0.66	288.15	50.00	34.242
4	39.83	1338.55	17.23	38.209	40.55	1323.96	15.02	37.857
5	39.83	761.77	1.03	8.853	40.55	757.21	1.03	8.885
6	39.83	711.81	1.03	7.454	40.55	709.22	1.03	7.521
7	39.83	581.76	1.02	4.256	40.55	581.76	1.02	4.334
8	39.83	475.14	1.01	2.164	40.55	477.32	1.01	2.241
9	3.97	306.43	86.82	0.053	3.96	306.43	86.82	0.053
10	3.97	565.76	84.21	1.548	3.96	565.76	84.21	1.545
11	3.97	571.76	84.21	4.398	3.96	571.76	84.21	4.387
12	39.18	690.54	17.50	15.498	39.90	672.07	15.22	14.859
13	3.97	306.03	0.05	0.469	3.96	306.03	0.05	0.467
14	3.97	306.03	0.05	0.018	3.96	306.03	0.05	0.018
15	268.26	289.15	1.01	0.672	266.93	289.15	1.01	0.669
16	268.26	289.15	1.37	0.682	266.93	289.15	1.37	0.678
17	268.26	296.03	1.33	0.797	266.93	296.03	1.33	0.793
18	187.78	288.15	1.01	0.292	186.85	288.15	1.01	0.291
19	4.92	288.15	1.01	0.012	4.89	288.15	1.01	0.012
20	190.02	299.51	1.01	0.370	189.07	299.51	1.01	0.369
21	2.68	289.15	1.01	0.007	2.67	289.15	1.01	0.007

Table A2
Stream data of small-scale hybrid power plants (inlet temperature of the combustion chamber: 800 °C).

Stream	Mercury 50				Mars100				GE10-1			
	Mass [kg/s]	Temperature [K]	Pressure [bar]	Exergy [MW]	Mass [kg/s]	Temperature [K]	Pressure [bar]	Exergy [MW]	Mass [kg/s]	Temperature [K]	Pressure [bar]	Exergy [MW]
1	18.03	288.15	1.01	0.028	41.73	288.15	1.01	0.065	42.48	288.15	1.01	0.066
2	17.94	577.78	9.45	5.005	41.73	690.54	17.50	16.503	42.48	672.07	15.22	15.820
3	17.94	288.15	9.09	7.862	0.30	288.15	50.00	15.379	0.28	288.15	50.00	14.828
4	17.94	1359.61	9.09	11.280	42.02	1338.04	17.23	39.275	42.76	1324.25	15.02	38.873
5	0.14	884.29	50.00	7.158	42.02	754.51	1.03	8.687	42.76	750.16	1.03	8.698
6	0.14	638.50	9.09	7.123	42.02	707.65	1.02	7.338	42.76	705.14	1.03	7.384
7	18.08	577.78	8.81	16.289	42.02	581.76	1.02	4.147	42.76	581.76	1.02	4.210
8	18.08	638.50	1.10	5.565	42.02	478.75	1.01	2.046	42.76	480.86	1.01	2.110
9	18.08	577.78	1.01	2.367	3.96	306.43	86.81	0.053	3.95	306.43	86.82	0.053
10					3.96	565.76	84.21	1.548	3.95	565.76	84.21	1.542
11					3.96	571.76	84.21	4.397	3.95	571.76	84.21	4.380
12					41.73	690.54	17.50	16.503	42.48	672.07	15.22	15.820
13					3.96	306.03	0.05	0.467	3.95	306.03	0.05	0.464
14					3.96	306.03	0.05	0.018	3.95	306.03	0.05	0.018
15					267.07	289.15	1.01	0.669	265.38	289.15	1.01	0.665
16					267.07	289.15	1.37	0.679	265.38	289.15	1.37	0.674
17					267.07	296.03	1.33	0.794	265.38	296.03	1.33	0.789
18					186.95	288.15	1.01	0.291	185.76	288.15	1.01	0.289
19					4.90	288.15	1.01	0.012	4.87	288.15	1.01	0.012
20					189.18	299.51	1.01	0.369	187.98	299.51	1.01	0.366
21					2.67	289.15	1.01	0.007	2.65	289.15	1.01	0.007

Table A3
Stream data of small-scale hybrid power plants (inlet temperature of the combustion chamber: 1000 °C).

Stream	Mercury 50				Mars100				GE10-1			
	Mass [kg/s]	Temperature [K]	Pressure [bar]	Exergy [MW]	Mass [kg/s]	Temperature [K]	Pressure [bar]	Exergy [MW]	Mass [kg/s]	Temperature [K]	Pressure [bar]	Exergy [MW]
1	18.49	288.15	1.01	0.029	43.19	288.15	1.01	0.067	43.97	288.15	1.01	0.068
2	18.40	577.78	9.45	5.134	43.19	690.54	17.50	17.082	43.97	672.07	15.22	16.375
3	18.40	288.15	9.09	8.063	0.08	288.15	50.00	4.398	0.07	288.15	50.00	3.633
4	18.40	1359.63	9.09	14.837	43.27	1338.37	17.23	39.966	44.04	1324.41	15.02	39.554
5	0.05	880.63	50.00	2.416	43.27	750.76	1.03	8.672	44.04	746.31	1.03	8.685
6	0.05	630.21	9.09	2.404	43.27	705.47	1.03	7.349	44.04	702.89	1.03	7.399
7	18.45	577.78	8.81	16.405	43.27	581.76	1.02	4.162	44.04	581.76	1.02	4.231
8	18.45	630.21	1.10	5.531	43.27	480.63	1.01	2.055	44.04	482.79	1.01	2.129
9	18.45	577.78	1.01	2.268	3.96	306.43	86.82	0.053	3.95	306.43	86.82	0.053
10					3.96	565.76	84.21	1.548	3.95	565.76	84.21	1.540
11					3.96	571.76	84.21	4.397	3.95	571.76	84.21	4.376
12					43.19	690.54	17.50	17.082	43.97	672.07	15.22	16.375
13					3.96	306.03	0.05	0.466	3.95	306.03	0.05	0.463
14					3.96	306.03	0.05	0.018	3.95	306.03	0.05	0.018
15					266.50	289.15	1.01	0.668	264.51	289.15	1.01	0.663
16					266.50	289.15	1.37	0.677	264.51	289.15	1.37	0.672
17					266.50	296.03	1.33	0.792	264.51	296.03	1.33	0.786
18					186.55	288.15	1.01	0.290	185.15	288.15	1.01	0.288
19					4.89	288.15	1.01	0.012	4.85	288.15	1.01	0.012
20					188.77	299.51	1.01	0.368	187.36	299.51	1.01	0.365
21					2.66	289.15	1.01	0.007	2.65	289.15	1.01	0.007

Table A4
Stream data of large-scale combined-cycle power plants (base simulations).

Stream	SGT5-4000F				SGT5-8000H			
	Mass [kg/s]	Temperature [K]	Pressure [bar]	Exergy [MW]	Mass [kg/s]	Temperature [K]	Pressure [bar]	Exergy [MW]
1	714.20	288.15	1.01	1.112	803.62	288.15	1.01	1.251
2	714.20	721.64	19.04	301.723	803.62	721.60	19.50	341.063
3	15.55	288.15	50.00	810.509	18.98	288.15	50.00	989.368
4	729.75	1547.56	18.77	873.908	822.61	1608.50	19.23	1045.978
5	729.75	850.44	1.03	215.897	822.61	890.71	1.03	272.086
6	729.75	757.80	1.03	164.922	822.61	776.26	1.03	199.081
7	729.75	581.76	1.02	82.279	822.61	581.76	1.02	94.565
8	729.75	435.94	1.01	32.247	822.61	419.98	1.01	33.361
9	100.05	306.43	86.82	1.339	125.38	306.43	86.82	1.678
10	100.05	565.76	84.21	39.060	125.38	565.76	84.21	48.950
11	100.05	571.76	84.21	110.954	125.38	571.76	84.21	139.047
12	714.20	721.64	19.04	301.723	803.62	721.60	19.50	341.063
13	100.05	306.03	0.05	12.372	125.38	306.03	0.05	15.784
14	100.05	306.03	0.05	0.463	125.38	306.03	0.05	0.580
15	7087.71	289.15	1.01	17.756	9048.14	289.15	1.01	22.667
16	7087.71	289.15	1.37	18.012	9048.14	289.15	1.37	22.994
17	7087.71	296.03	1.33	21.066	9048.14	296.03	1.33	26.893
18	4961.40	288.15	1.01	7.723	6333.70	288.15	1.01	9.859
19	129.96	288.15	1.01	0.325	165.90	288.15	1.01	0.414
20	5020.48	299.51	1.01	9.789	6409.12	299.51	1.01	12.496
21	70.88	289.15	1.01	0.178	90.48	289.15	1.01	0.227

Table A5
Stream data of large-scale hybrid power plants (inlet temperature of the combustion chamber: 800 °C).

Stream	SGT5-4000F				SGT5-8000H			
	Mass [kg/s]	Temperature [K]	Pressure [bar]	Exergy [MW]	Mass [kg/s]	Temperature [K]	Pressure [bar]	Exergy [MW]
1	748.99	288.15	1.01	1.166	841.46	288.15	1.01	1.310
2	748.99	721.64	19.04	316.423	841.46	721.60	19.50	357.122
3	9.70	288.15	50.00	505.549	12.40	288.15	50.00	646.245
4	758.69	1547.56	18.77	886.147	853.86	1608.51	19.23	1058.597
5	758.69	842.24	1.03	209.976	853.86	882.12	1.03	264.672
6	758.69	753.82	1.03	160.651	853.86	772.37	1.03	193.813
7	758.69	581.76	1.02	78.476	853.86	581.76	1.02	89.773
8	758.69	439.54	1.01	28.369	853.86	423.57	1.01	28.394
9	99.68	306.43	86.82	1.334	125.04	306.43	86.82	1.673
10	99.68	565.76	84.21	38.916	125.04	565.76	84.21	48.819
11	99.68	571.76	84.21	110.542	125.04	571.76	84.21	138.673
12	748.99	721.64	19.04	316.423	841.46	721.60	19.50	357.122
13	99.68	306.03	0.05	12.280	125.04	306.03	0.05	15.683
14	99.68	306.03	0.05	0.461	125.04	306.03	0.05	0.579
15	7033.72	289.15	1.01	17.620	8989.20	289.15	1.01	22.519
16	7033.72	289.15	1.37	17.875	8989.20	289.15	1.37	22.844
17	7033.72	296.03	1.33	20.906	8989.20	296.03	1.33	26.718
18	4923.61	288.15	1.01	7.664	6292.44	288.15	1.01	9.795
19	128.97	288.15	1.01	0.322	164.82	288.15	1.01	0.412
20	4982.24	299.51	1.01	9.714	6367.37	299.51	1.01	12.415
21	70.34	289.15	1.01	0.176	89.89	289.15	1.01	0.225

Table A6
Stream data of large-scale hybrid power plants (inlet temperature of the combustion chamber: 1000 °C).

Stream	SGT5-4000F				SGT5-8000H			
	Mass [kg/s]	Temperature [K]	Pressure [bar]	Exergy [MW]	Mass [kg/s]	Temperature [K]	Pressure [bar]	Exergy [MW]
1	771.34	288.15	1.01	1.200	865.77	288.15	1.01	1.347
2	771.34	721.64	19.04	325.864	865.77	721.60	19.50	367.439
3	5.95	288.15	50.00	309.902	8.19	288.15	50.00	426.702
4	777.29	1547.56	18.77	895.042	873.96	1608.47	19.23	1067.806
5	777.29	837.17	1.03	207.237	873.96	876.79	1.03	261.046
6	777.29	751.34	1.03	158.929	873.96	769.93	1.03	191.515
7	777.29	581.76	1.02	77.053	873.96	581.76	1.02	87.779
8	777.29	441.77	1.01	26.905	873.96	425.81	1.01	26.296
9	99.44	306.43	86.82	1.331	124.82	306.43	86.82	1.670
10	99.44	565.76	84.21	38.822	124.82	565.76	84.21	48.734
11	99.44	571.76	84.21	110.276	124.82	571.76	84.21	138.432
12	771.34	721.64	19.04	325.864	865.77	721.60	19.50	367.439
13	99.44	306.03	0.05	12.221	124.82	306.03	0.05	15.619
14	99.44	306.03	0.05	0.460	124.82	306.03	0.05	0.578
15	6999.56	289.15	1.01	17.535	8951.93	289.15	1.01	22.426
16	6999.56	289.15	1.37	17.788	8951.93	289.15	1.37	22.749
17	6999.56	296.03	1.33	20.804	8951.93	296.03	1.33	26.607
18	4899.69	288.15	1.01	7.627	6266.35	288.15	1.01	9.754
19	128.34	288.15	1.01	0.321	164.14	288.15	1.01	0.410
20	4958.04	299.51	1.01	9.667	6340.97	299.51	1.01	12.363
21	70.00	289.15	1.01	0.175	89.52	289.15	1.01	0.224

References

- [1] Antonanzas J, Jimenez E, Blanco J, Antonanzas-Torres F. Potential solar thermal integration in Spanish combined cycle gas turbines. *Renew Sustain Energy Rev* 2014;37:36–46. <http://dx.doi.org/10.1016/j.rser.2014.05.006>.
- [2] Peterseim JH, White S, Tadros A, Hellwig U. Concentrated solar power hybrid plants, which technologies are best suited for hybridisation? *Renew Energy* 2013;57:520–32. <http://dx.doi.org/10.1016/j.renene.2013.02.014>.
- [3] Manente G. High performance integrated solar combined cycles with minimum modifications to the combined cycle power plant design. *Energy Convers Manage* 2016;111:186–97. <http://dx.doi.org/10.1016/j.enconman.2015.12.079>.
- [4] Amelio M, Ferraro V, Marinelli V, Summaria A. An evaluation of the performance of an integrated solar combined cycle plant provided with air-linear parabolic collectors. *Energy* 2014;69:742–8. <http://dx.doi.org/10.1016/j.energy.2014.03.068>.
- [5] Buck R, Giuliano S, Uhlig R. Central tower systems using the Brayton cycle. Elsevier Ltd; 2017. <http://dx.doi.org/10.1016/B978-0-08-100516-3.00016-2>.
- [6] Alqahtani BJ, Patiño-Echeverri D. Integrated solar combined cycle power plants: paving the way for thermal solar. *Appl Energy* 2016;169:927–36. <http://dx.doi.org/10.1016/j.apenergy.2016.02.083>.
- [7] Saghaifir M, Gadalla M. Thermo-economic analysis of conventional combined cycle hybridization: United Arab Emirates case study. *Energy Convers Manage* 2016;111:358–74. <http://dx.doi.org/10.1016/j.enconman.2015.12.016>.
- [8] Korzynietz R, Brioso JA, Del Río A, Quero M, Gallas M, Uhlig R, et al. Solugas – comprehensive analysis of the solar hybrid Brayton plant. *Sol Energy* 2016;135:578–89. <http://dx.doi.org/10.1016/j.solener.2016.06.020>.
- [9] Karni J R, Kribus A, Doron P, Rubín R, Fiterman A, Sagie D, et al. The DIAPR: a high-pressure, high-temperature solar receiver. *J Sol Energy Eng* 1997;119. <http://dx.doi.org/10.1115/1.2871853>.
- [10] Buck R, Bräuning T, Denk T, Pfänder M, Schwarzbözl P, Tellez F. Solar-hybrid gas turbine-based power tower systems (REFOS). *J Sol Energy Eng* 2002;124:2. <http://dx.doi.org/10.1115/1.1445444>.
- [11] Ávila-Marín AL. Volumetric receivers in solar thermal power plants with central receiver system technology: a review. *Sol Energy* 2011;85:891–910. <http://dx.doi.org/10.1016/j.solener.2011.02.002>.
- [12] Spelling J, Favrat D, Martin A, Augsburg G. Thermo-economic optimization of a combined-cycle solar tower power plant. *Energy* 2012;41:113–20. <http://dx.doi.org/10.1016/j.energy.2011.03.073>.
- [13] Heller P, Pfänder M, Denk T, Tellez F, Valverde A, Fernandez J, et al. Test and evaluation of a solar powered gas turbine system. *Sol Energy* 2006;80:1225–30.

- <http://dx.doi.org/10.1016/j.solener.2005.04.020>.
- [14] Pozivil P, Aga V, Zagorskiy A, Steinfeld A. A pressurized air receiver for solar-driven gas turbines. *Energy Procedia* 2013;49:498–503. <http://dx.doi.org/10.1016/j.egypro.2014.03.053>.
- [15] Del Río A, Korzynietz R, Brioso JA, Gallas M, Ordóñez I, Quero M. Soltrec – pressurized volumetric solar air receiver technology. *Energy Procedia* 2015;69:360–8. <http://dx.doi.org/10.1016/j.egypro.2015.03.042>.
- [16] SteagEnergyServices. EBSILONProfessional; 2016. < http://www.steag-systemtechnologies.com/ebsilon_professional.html > [accessed February 21, 2012].
- [17] Solar Turbines Inc. Data Sheet, Mars100 – Solar turbines; 2012.
- [18] General Electric – Oil & Gas. Data Sheet, GE10-1 Gas Turbine; 2005.
- [19] Office of Industrial Technologies, Energy Efficiency, and Renewable Energy; Department of Energy. Solar Mercury 50 Gas Turbine – Project fact sheet; 1999.
- [20] Kalina J. Comparative analysis of alternative configurations of the mercury 50 recuperated gas-turbine-based biomass integrated gasification combined heat and power (BIGCHP) plant. *Energy Fuels* 2012;26:6452–565.
- [21] Bolland O. Thermal power generation 2010.
- [22] Schmitz M, Schwarzbözl P, Buck R, Pitz-Paal R. Assessment of the potential improvement due to multiple apertures in central receiver systems with secondary concentrators. *Sol Energy* 2006;80:111–20. <http://dx.doi.org/10.1016/j.solener.2005.02.012>.
- [23] SOLGATE Report, Ormat, Ciemat, Dlr, Solucar, Tuma. Solar hybrid gas turbine electric power system; 2005. ISBN 92-894-4592-0.
- [24] U.S. DOE. SunShot vision study. 2012; 2012.
- [25] Pacheco JE, Reilly HE, Kolb GJ, Tyner CE. Summary of the solar two test and evaluation program; 2000.
- [26] NREL NREL, LLC A for SE, DOE USDOE. System Advisor Model (SAM); 2015.
- [27] Wagner MJ. Simulation and predictive performance modeling of utility-scale central receiver system power plants. 2008; 2008. p. 259.
- [28] Huang W, Xu Q. Development of an analytical method and its quick algorithm to calculate the solar energy collected by a heliostat field in a year. *Energy Convers Manage* 2014;83:110–8. <http://dx.doi.org/10.1016/j.enconman.2014.03.065>.
- [29] NREL. Integrated Layout and Optimization Tool for Solar Power Towers | Concentrating Solar Power | NREL; 2017. < <https://www.nrel.gov/csp/solarpilot.html> > [accessed April 4, 2017].
- [30] Wagner MJ. Optimization of stored energy dispatch for concentrating solar power systems. Colorado School of Mines, Arthur Lakes Library; 2017.
- [31] Dellin TA. An improved hermite expansion calculation of the flux distribution from heliostats: SAND79-8619. Livermore, CA. 1979; 1979.
- [32] Petela R. Exergy of undiluted thermal radiation. *Sol Energy* 2003;74:469–88. [http://dx.doi.org/10.1016/S0038-092X\(03\)00226-3](http://dx.doi.org/10.1016/S0038-092X(03)00226-3).